



## **NUMERICAL STUDY OF THE SOIL-STRUCTURE INTERACTION DURING STRONG EARTHQUAKES**

**Roberto O. CUDMANI<sup>1</sup>, Roberto CUDMANI<sup>2</sup>**

### **SUMMARY**

The non linear dynamic soil-structure interaction of three reinforcement concrete building frames (3, 6, and 12 levels) subjected to strong earthquakes is studied using the FEM. The soil behaviour is modelled with hypoplastic and visco-hypoplastic relations which are able to model the response of cohesionless and cohesive soils under alternating and dynamic loading, for drained and undrained conditions. The behaviour of reinforced concrete is modelled using an elastic-plastic constitutive law for the plain concrete and elastic-ideal plastic for the steel bars. It is assumed that the buildings are founded on a layered ground from Treasure Island, San Francisco Bay (Seed et al., 1991). An acceleration record at Yerba Buena Island during the Loma Prieta 1989 earthquake is used as bedrock excitation. In order to quantify the influence of the soil-structure interaction, the ground motion at the foundation depth due to the bedrock excitation is first calculated without considering the structure ("free field acceleration"). This ground motion is then applied to the base of the buildings to evaluate the internal forces and deflections of the structure. In a third analysis, the dynamic response of both structure and soil due to the same bedrock excitation is considered. Based on the comparison of the numerical results it is concluded that the proposed numerical model is a powerful tool to quantify the influence of soil-structure interaction on the response of buildings during strong earthquakes.

### **1 INTRODUCTION**

In earthquake engineering practice, seismic design of building structures is based on the recommendations of seismic codes. Despite the complex nature of the phenomena and due to the difficulty to identify and quantify the many variables controlling the seismic response of a structure codes adopt substantial and partly crude approximations to provide simple frameworks for design.

For instance, for buildings with a height/width relation  $H/B$  lower than 4 an "equivalent" static analysis is proposed by the code INPRES-CIRSOC 103 (Argentina). The equivalent static force to be applied to the base of the structure depends on a expected pseudo-acceleration, the fundamental period of the structure in the elastic regime and the mass of the building as well as on correction factors taking into account the ductility of the structure, i.e. its capacity to dissipate energy in the plastic regime. The equivalent static

---

<sup>1</sup> Senior Research Assistant, Institute of Soil and Rock Mechanics, University of Karlsruhe, Germany

<sup>2</sup> Professor, Department of Structural Engineering, National University of Tucumán, Argentina

force at the base is distributed throughout the height of the building according to the shape of the first mode of vibration. The response spectra used for the evaluation of the pseudo-acceleration are determined for a viscous-elastic one-degree of freedom system using acceleration records from past earthquakes or obtained synthetically. The influence of the soil is taken into account by using different response spectra for different soil types.

For higher buildings the codes recommend the use of the spectral modal analysis (a more sophisticated equivalent static analysis) or the step-by-step modal superposition analysis in order to take into account higher modes of vibration in the evaluation of the seismic response of the structure. Obviously, these methods can at best crudely consider the influence of the soil, but they neglect the influence of the soil-structure interaction (SSI) on the dynamic response of the structure completely.

Based on the results of simplified analysis, in which viscous-elastic behaviour of the soil and the structure is usually assumed, many seismic codes suggest that neglecting SSI has a beneficial effect for seismic response and leads to an improvement of safety margins. This assumption has been corroborated for buildings founded on very stiff soils and rock, whose behaviour can be roughly approximated by visco-elastic models. However, despite extensive research in the past three decades, there is still a lack of knowledge regarding the role of SSI in the seismic response of structures on soft or even liquefiable soils, especially in the case of strong earthquakes where non-linear soil behaviour predominates.

In the authors' opinion the Finite Element Method (FEM) is the most appropriate tool for investigating SSI if non-linear behaviour of the soil and structure is to be considered. However, due to the difficulties associated with the description of the complex soil and structure material behaviour, as well as the unbounded nature of the soil medium, the FE simulation of the SSI still remains a challenge (Mylonakis and Gazetas, 2000).

The aim of this contribution is to develop a FE model for the investigation of the SSI of reinforced concrete (RC) structures founded on soft or even liquefiable soils in order to quantify the effect of considering SSI in the seismic design of buildings subjected to strong earthquakes. It is noted that the scope of this work is to highlight rather than fully solve this complex issue. The dynamic response of three RC frames for 3-, 6- and 12 storey-buildings founded on a liquefiable soil during the Loma Prieta 1989 earthquake is analysed. For the study a layered soil profile from Treasure Island, San Francisco Bay is adopted. In Section 2 the pre-dimensioning of the RC structures following the equivalent static method adopted by the Argentinian seismic code INPRES-CIRSOC 103 is carried out. In Section 3 the dynamic behaviour of a rigid block on a thin soil layer subjected to base shaking is analysed in order to introduce the hypoplastic constitutive relations and to illustrate the most relevant features of non-linear soil behaviour during strong earthquakes. A one-dimensional ground response model based on the same constitutive relations is introduced in Sections 4. This model is used to generate the input motions ("base shaking") for the FE simulations from the accelerations recorded at a rock outcrop in Yerba Buena Island, near Treasure Island during the Loma Prieta Earthquake. The constitutive relation for RC is briefly introduced in section 5. The FE models are developed in Section 6, and the dynamic analysis of the three structures with and without consideration of influence of the SSI is carried out in Section 7.

## **2 PRE-DIMENSIONING OF THE RC-STRUCTURE OF THE BUILDINGS**

It is assumed that the structure of the buildings consists of parallel RC frames. The geometry, material properties and gravitational loads of the frames are listed in Table 1.

As a first step the dimensions of beams and columns of the frames were estimated by considering only gravitational loads and a reduced compressive strength of concrete (15 MPa). As a second step equivalent static forces were determined according to the INPRES-CIRSOC 103 seismic code. This code divides the country in five seismic zones (0: very low ,4: very high seismic hazard). It was assumed that an earthquake as the Loma Prieta 1989 can be expected in the Seismic Zone 3 which is characterized by the pseudo-acceleration spectra shown in Fig. 1. A soil named type II was adopted (soil with intermediate stiffness,

shear wave velocity 100-400 m/s). The internal forces and moments in beams and columns were calculated by superposing the equivalent horizontal forces and the gravitational loads including the weight of structural elements.

Table 1. Geometry, material properties and gravitational loads of the RC frames.

foundation depth	-3.5 m
height of storeys	3.0 m
length of the frame in the direction of motion	6.0 m
distance between the frames	5.0 m
load on beams (without beam weight)	29 kN/m
compressive strength of the concrete	20 MPa
yield stress of steel	420 MPa

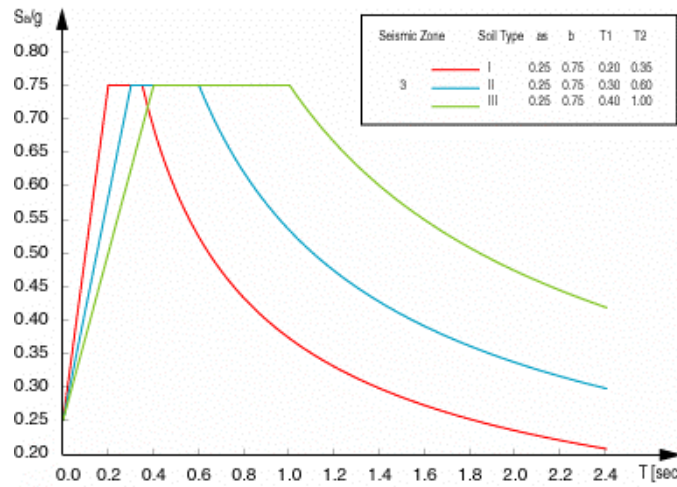


Figure 1. Pseudo-acceleration spectra for Seismic Zone 3 according to INPRES-CIRSOC 103.

### 3 HYPOPLASTIC AND VISCO-HYPOPLASTIC CONSTITUTIVE RELATIONS

For introducing the concept of hypoplasticity and to better understand the role of soil in SSI, a block upon a horizontal shaking base with a thin dry granular layer in between has been considered (Fig.3a). The mass of the block is  $m_a$ . The plane is excited with an harmonic acceleration  $a = a_0 \cos \omega t$ , where  $a_0$  is the amplitude of the acceleration and  $u_0 = -a_0/\omega^2$  is the amplitude of the displacement of the plane. Simple shearing is assumed to occur, i.e. lateral squeezing out may be prevented. In the normal direction, the initial pressure  $\sigma_z$  is given by the weight  $m_a g$  of the block. The horizontal pressures are  $\sigma_x = \sigma_y = K \sigma_z$  with an earth pressure coefficient  $K$ . The height  $h$  of the layer changes together with the void ratio  $e$ , its initial value  $e_0$  may correspond to a rather loose packing.  $h$  decreases from  $h_0$  due to shaking,  $h_0/(1+e_0) = h/(1+e)$  expresses conservation of solid mass with constant grain volume. An absolute Cartesian co-ordinate system  $X, Y, Z$  (capital letters) and a local co-ordinate system  $x, y, z$  fixed to the plane are defined. Since the block is rigid and no rotations are allowed for, the position of the block at time  $t$  in the local and global co-ordinate systems is defined respectively by the coordinates  $(x(t), y(t), z(t))$  and  $(X(t), Y(t), Z(t))$  of any point belonging to the block (for instance the center of the block). The absolute displacement of the block at time  $t$  is defined by  $u_x(t) = X(t) - X(t=0)$ . The motion of the block is described by two coupled differential equations, which have been integrated numerically using an implicit Newmark procedure (Gudehus et al., 2004).

Vertical and horizontal forces acting on the block,  $T_z$  and  $T_x$ , are proportional to the vertical and shear stresses  $\sigma_z$ ,  $\tau_{xz}$  in the sand layer.  $\tau_{xz}$  and  $\sigma_z$  are calculated by integrating the hypoplastic constitutive equa-

tion as a function of the non-zero strain rates  $\dot{\gamma} = \dot{\gamma}_{xz}$  and  $\dot{\epsilon} = \dot{\epsilon}_z$  and the current material state. The strain rates are related to the components  $\dot{x}$  and  $\dot{z}$  of the relative velocity  $v$  of the block through the compatibility conditions  $\dot{\gamma} = \dot{x}/h$  and  $\dot{\epsilon} = \dot{z}/h$ .

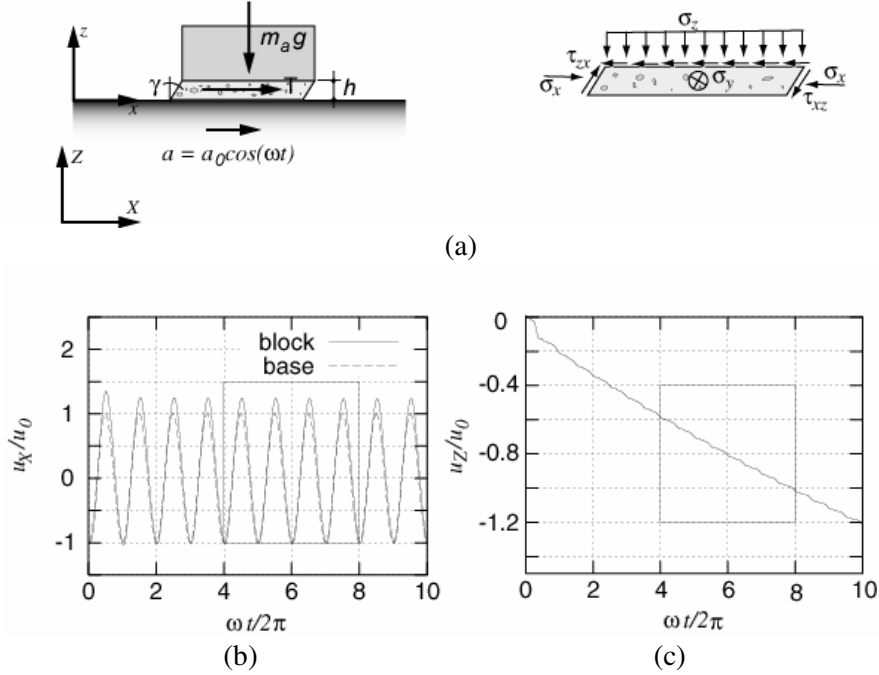


Figure 2 (a) Block (mass per  $m^2$   $m_a=10$   $t/m^2$ ) upon a laterally confined freely dilating granular layer with constant vertical stress  $\sigma_z = m_a g = 100$  kPa, initial horizontal stresses  $\sigma_x = \sigma_y = 0.5\sigma_z$  and initial relative density  $I_d=0.25$ . Calculation with  $a_0=0.3g$  and  $f=3$  Hz. (b) Horizontal displacements of the base and the block, (c) Vertical displacement of the block versus number of shaking cycles.

Results of a calculation are shown in Fig. 2b and c. The horizontal block motion  $u_x$  is retarded and not harmonic,  $|u_x| > |u_0|$  indicates amplification. Due to densification of the sand layer the block moves stepwise downwards. This occurs with a frequency which is twice that of the base (it cannot be seen in the figure), and with an oscillation amplitude which does not exceed 10% of  $u_0$ . Both densification and rate of increase of permanent displacements  $u_z$  decrease with further cycles.

The calculated evolutions of shear stress  $\tau$  and void ratio  $e$  are plotted in Fig. 3a and b as functions of  $\gamma$ . For the 30<sup>th</sup> cycle the layer is stiffer and denser and the hysteresis smaller than for the 2<sup>nd</sup> cycle. With two reversals of  $\gamma$  the density goes through four reversals. In other words, one shear cycle induces nearly two dilatancy cycles (without change of pressure), as can also be seen in Fig. 3b.

Fig. 3c shows the normalized shear stiffness  $G/G_{max}$  and the damping ratio  $D$  versus  $\log \gamma$  predicted by the hypoplastic constitutive law for a quartz sand layer subjected to strain-controlled simple shear. The initial relative density is  $I_d=0.50$  and the initial pressures are  $\sigma_z=100$  kPa and  $\sigma_x = \sigma_y = 50$  kPa.  $G$  and  $D$  are defined as  $G=\tau_a/\gamma_a$  and  $D=A/2\pi \tau_a \gamma_a$ , where  $\tau_a$  and  $\gamma_a$  are the stress and strain amplitudes, and  $A$  is the area of the hysteresis loop in the  $\tau, \gamma$ -plane. The maximum shear stiffness  $G_{max} = \tau_a/\gamma_a$  holds for  $\gamma_a \rightarrow 0$ . As can be seen, the familiar decrease of  $G/G_{max}$  and increase of  $D$  with  $\log \gamma$  are obtained.

The constitutive equation is written as a tensor-valued function of the stress rate depending on effective stress, void ratio and strain rate. The relation describes plastic deformations of a solid skeleton under monotonic as well as cyclic loading. It incorporates the critical state concept of soil mechanics and the dependence of the stiffness on current stress, density and history of deformation. The extremely variable

strength and stiffness values are thus *derived* and not assumed in advance as with other constitutive relations.

For rate independent materials, the rate of the effective stress  $\dot{\boldsymbol{\sigma}}'$  is determined by the rate of strain  $\dot{\boldsymbol{\epsilon}}$ , the current effective stress  $\boldsymbol{\sigma}'$ , the void ratio  $e$  and the so-called intergranular strain tensor  $\boldsymbol{\delta}$  which takes into account the influence of the recent deformation history:

$$\dot{\boldsymbol{\sigma}}' = \mathbf{H}(\boldsymbol{\sigma}', e, \boldsymbol{\delta}, \dot{\boldsymbol{\epsilon}}) \quad (1)$$

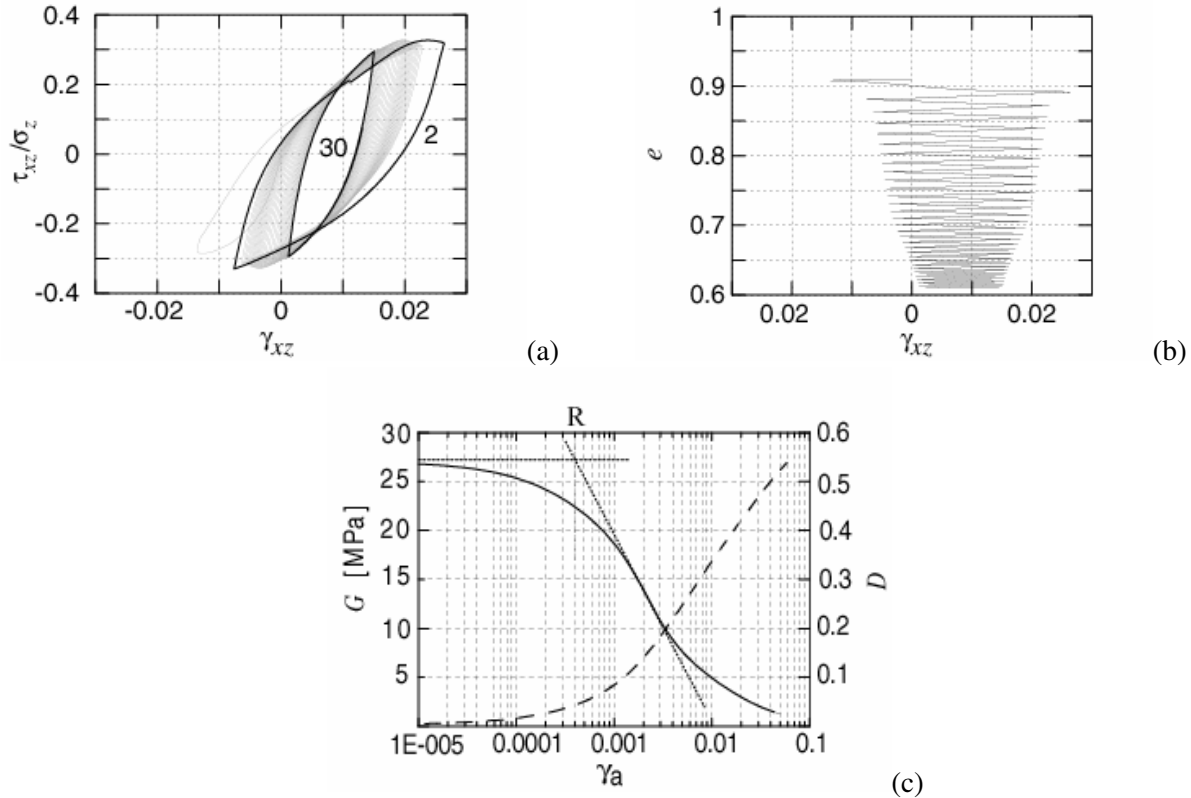


Figure 3 (a) Normalized shear stress versus shear strain of the granular layer of Fig. 3(b) Evolution of the void ratio. (c) Normalized shear stiffness and damping ratio versus amplitude  $\gamma_a$  of  $\gamma$

Fig. 4a shows the motion of a block on a thin soil layer as in Fig. 2, but now with water saturation and without drainage. The layer height  $h$  is constant, and so is the total vertical pressure  $\sigma$ . Effective (or skeleton) pressure  $\sigma'$  and pore water pressure  $p_w$  are variable with  $\sigma = \sigma' + p_w$ . As can be seen in Fig. 4a, b and c, shear stiffness, shear amplitude and mean effective pressure  $p'$  decrease with the number of cycles.  $p'$  oscillates with twice the frequency of the base. After a certain number of cycles that depends on the initial shear amplitude, the normal stress and the void ratio, the block stands almost still on a nearly liquefied layer. This effect, which is called *layer separation*, was used in the ancient Japanese seismic isolation known as Hanchiku with saturated loose sand layers embedded in fat clay (Pralle et al., 2000).

Saturated soils with soft particles (e.g. clays) showing rate-dependence are modelled by a visco-hypoplastic relation. The effective stress rate  $\dot{\boldsymbol{\sigma}}'$  is again a tensor-valued function of the rate of strain  $\dot{\boldsymbol{\epsilon}}$ , the current effective stress  $\boldsymbol{\sigma}'$ , the void ratio  $e$ , the intergranular strain tensor  $\boldsymbol{\delta}$  and a non-linear viscous strain rate tensor  $\dot{\boldsymbol{\epsilon}}_v$  as an additional variable:

$$\dot{\boldsymbol{\sigma}}' = \mathbf{H}(\boldsymbol{\sigma}', e, \boldsymbol{\delta}, \dot{\boldsymbol{\epsilon}}, \dot{\boldsymbol{\epsilon}}_v) \quad (2)$$

For constant strain rate it comes up to a modified Cam Clay model. Viscous effects become relevant if an overconsolidation ratio  $OCR$  (that depends on  $e, p'$  and a shear stress ratio  $\tau/p'$ ) is lower than ca. 1.4. Viscous effects increase with a viscosity index  $I_v$  that ranges from 0.02 to 0.06 for hard and soft clay minerals. For  $OCR$  greater than ca. 1.4 the response becomes hypoplastic.

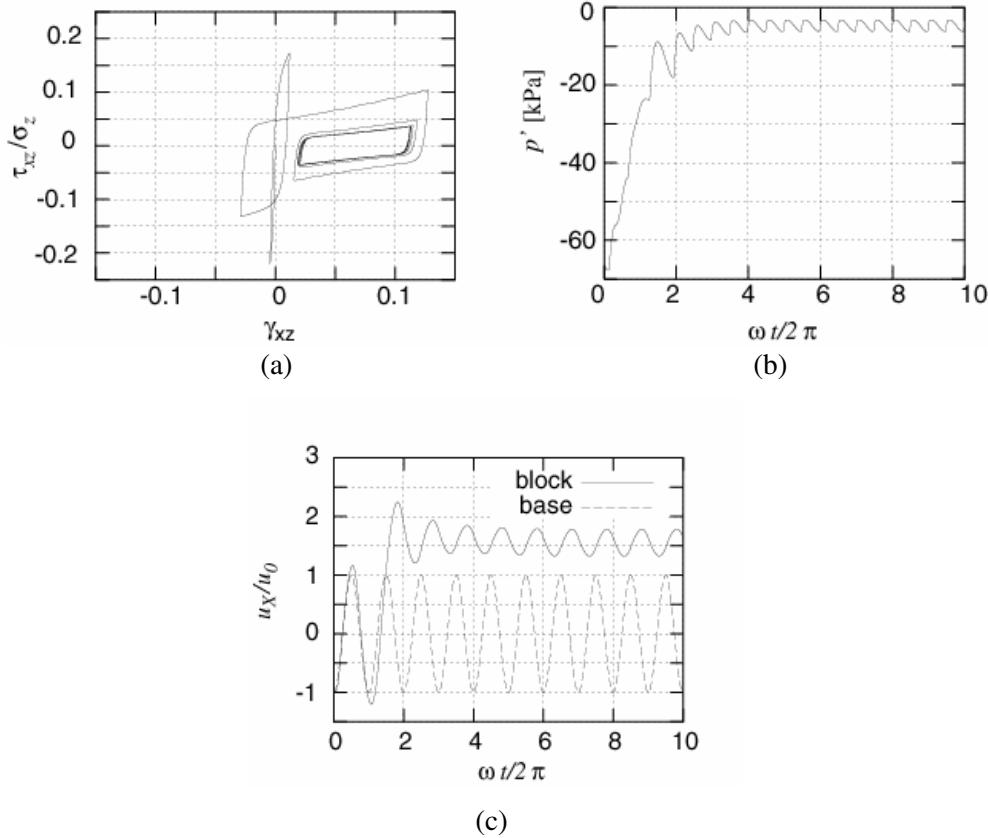


Figure 4 Block upon a thin saturated sand layer without drainage and a harmonically shaking base. (a) Evolution of shear stress versus shear strain, (b) mean effective pressure and Horizontal displacements of the base and the block (c) versus time. Calculated with  $a_0=0.3$  g and  $f=3$  Hz, and with the same initial state as shown in Fig. 3 except for the relative density  $I_d=0.5$ .

As distinct from elastoplasticity theories, the description of the plastic deformation through equations (1), (2) does not require the introduction of a yield surface and a flow rule, nor the decomposition of the deformation into elastic and plastic parts. A detailed description of the hypoplastic relations (1), (2) can be found in Niemunis (2003). The material parameters are rather easily determined or estimated from granulometric properties (Gudehus and Herle, 1999). The initial state, i.e. stress, void ratio and intergranular strain, must be known for any application. The initial void ratio can be determined directly from “undisturbed” soil samples or estimated indirectly from in-situ tests. For this purpose, a procedure for the interpretation of cone penetration and pressuremeter tests based on a hypoplastic cavity expansion model can be applied (Cudmani and Osinov, 2001). The initial stress state is determined from the weight of the overlying soil strata and assumed earth pressure coefficients. The initial value of the intergranular strain tensor does not play an important role because the influence of this value vanishes after one or two cycles.

For a block on a thin saturated layer of soil with soft particles base shaking leads to a quantitatively different response which may be briefly indicated without further drawings. The displacement amplitude of

the block is bigger due to the lower stiffness of soft soils and the only moderate reduction of the effective pressure  $p'$ . As OCR increases with the decrease of  $p'$  the response after one or two strong cycles becomes nearly hypoelastic. Close to a certain frequency the oscillation amplitude is markedly amplified. Only if the soil was already close to a limit state prior to shaking, for example a slope close to static failure, viscous effects do become marked. This leads to creep after shaking which comes to an end only if densification is enabled by drainage.

#### 4 NUMERICAL MODEL FOR GROUND RESPONSE ANALYSIS

An *effective-stress level ground response analysis* based on the numerical solution of a nonlinear one-dimensional wave propagation problem was developed by Osinov (2003). The motion of the soil deposit in this model is induced by a plane wave coming from below.

For the part of the layer above the water table, the governing system of equations consists of the equations of motion, the constitutive equation for the solid skeleton, and the mass balance equation for the void ratio. For the soil below the water table, the stress  $\sigma'$  in (1) represents the effective stress, and pore pressure is introduced as an additional variable with an appropriate constitutive relation. The latter involves the compressibility of the pore fluid which depends strongly on the degree of saturation.

In the case of drained conditions, the so-called  $u-p$  formulation (Zienkiewicz et al., 1980; Zienkiewicz et al., 1999) was used for the present study. This formulation constitutes an approximation to the dynamic equations for a two-phase medium which allows seepage of the pore fluid to be taken into account. The boundary condition at the base of the layer consists of the velocity components as functions of time. In addition, if the soil is saturated, this boundary is assumed to be impermeable. The upper boundary of the layer is free of traction. The pore pressure at the water table is taken to be constant (zero). The problem is solved numerically by a finite-difference algorithm with implicit time integration.

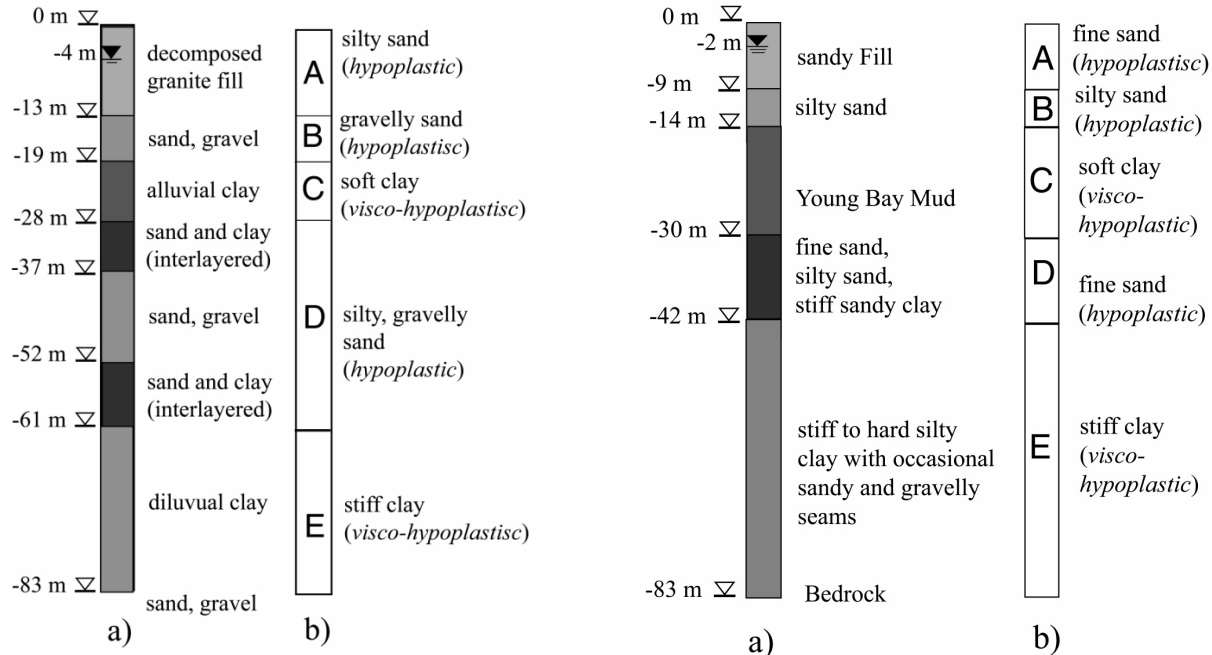


Figure 5. Port Island (left) and Treasure Island (right): real (a) and idealized (b) soil profiles.

In order to verify the applicability of the proposed numerical model to real seismic events the dynamic response at of two level ground sites during the Kobe 1995 and Loma Prieta 1989 earthquakes were analysed by Cudmani et al. (2003).

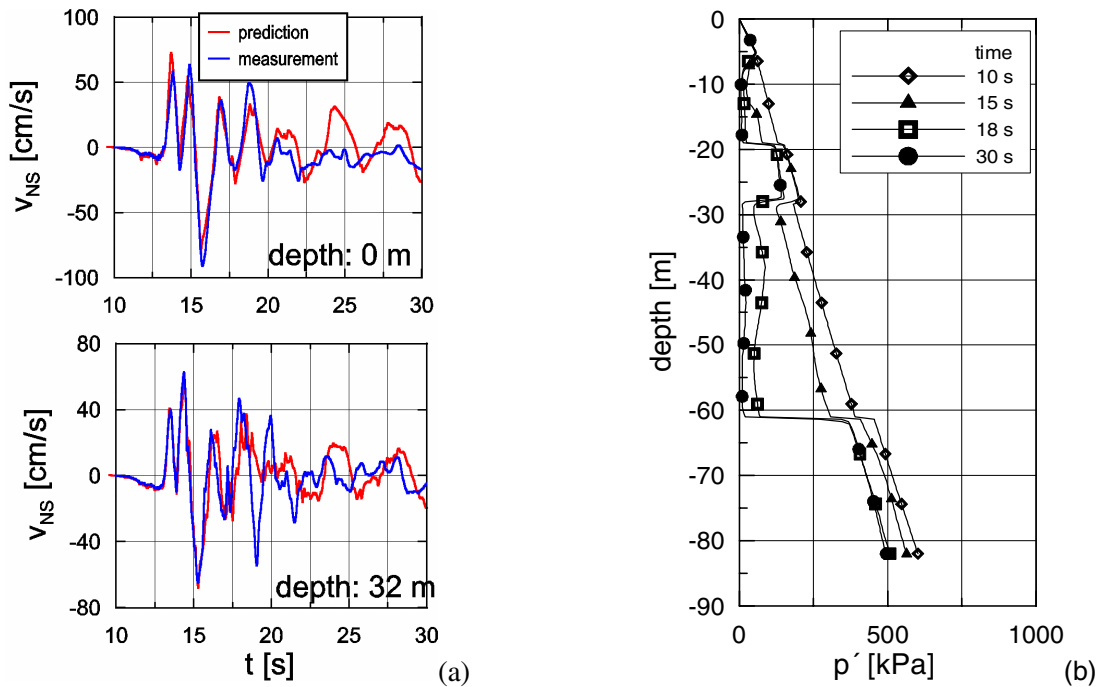


Figure 6. Kobe Port Island: (a) Measured and predicted velocities at the surface and at depths of 0 and 32 m in the North-South direction. (b) Calculated distribution of the mean effective stresses over depth during the earthquake (Cudmani et al., 2003).

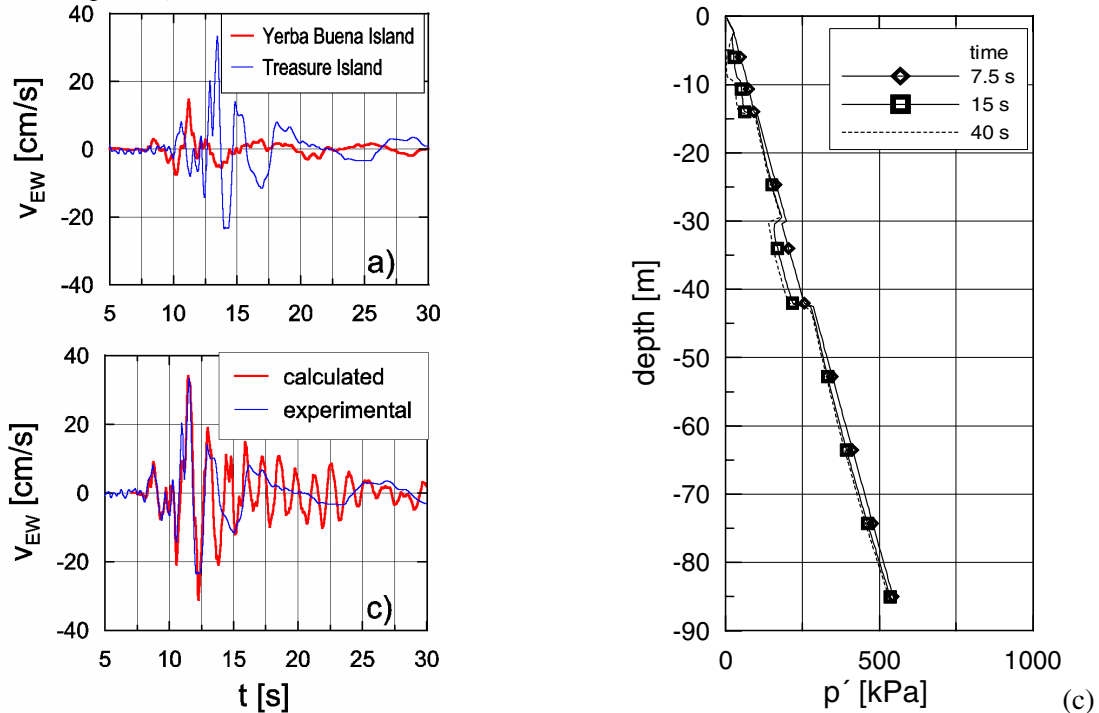


Figure 7. Treasure Island: (a) Measured E-W velocity components at the surface and at the bedrock. (c) Experimental and predicted velocities at the surface in the E-W direction. (d) Calculated distribution of the mean effective stresses over depth during the earthquake (Cudmani et al. 2003).

The soil profiles at the considered sites (Kobe Port Island and Treasure Island, respectively) were replaced by some layers with viscoplastic or visco-hypoplastic behaviour (s. Fig. 5a and b).

The parameters were estimated from granulometric properties of the layers. The void ratios in the cohesionless soil layers were determined from SPT data. The initial void ratio in the cohesive soil layers is calculated with the constitutive law assuming OCR =1. Using an acceleration record for 83 m depth from the 1995 Hyagoken-Nanbu earthquake the one-dimensional dynamic response of a soil profile was calculated. As shown in Fig. 6a, the calculated and measured horizontal velocities nearly coincide for the three considered depths. The same good agreement was obtained with data from San Francisco for the 1989 Loma Prieta earthquake (Fig. 7a). The calculations also show that liquefaction occurred in both cases, but it was stronger at the Port Island site (Fig. 6b and 7b).

## 5 CONSTITUTIVE MODELS FOR CONCRETE AND REINFORCEMENT

In order to include non-linear behaviour of the structure in the numerical study of the SSI, the mechanical behavior of the concrete was simulated using a damage plasticity constitutive model included in the ABAQUS FE-program. The model is based on the constitutive relations by Lubliner et al. (1989) and by Lee and Fenves (1998), and can be applied to the analysis of concrete structures under cyclic and/or dynamic loading. It captures the effects of irreversible damage associated with the failure mechanisms that occur in concrete and other quasi-brittle materials under fairly low confining pressures (less than four or five times the ultimate compressive stress in uniaxial compression loading). These effects manifest themselves in the following macroscopic properties:

- different yield strengths in tension and compression, with the initial yield stress in compression ten times higher than the initial yield stress in tension or more;
- softening behavior in tension as opposed to initial hardening followed by softening in compression;
- different degradation of the elastic stiffness in tension and compression;
- stiffness recovery effects during cyclic loading; and
- rate sensitivity, especially an increase of the peak strength with strain rate.

The stress-strain relations are governed by scalar damaged elasticity. For uniaxial compression (sub-index  $c$ ) and tension (sub-index  $t$ ):

$$\sigma_{t,c} = (1 - d_{t,c})E_0(\varepsilon - \varepsilon^{pl})$$

$E_0$  is the initial (undamaged) elastic stiffness of the material;  $E = E_0(1 - d_{t,c})$  is the degraded elastic stiffness; and  $d_t$  and  $d_c$  are scalar stiffness degradation variables, which can take values in the range from zero (undamaged material) to one (fully damaged material). Therefore damage associated with the failure mechanisms of the concrete (cracking and crushing) results in a reduction in the elastic stiffness. An effective stress is defined as:

$$\bar{\sigma}_{t,c} = E_0(\varepsilon - \varepsilon^{pl})$$

The Cauchy stress is related to this effective stress through the scalar degradation relation:

$$\bar{\sigma}_{t,c} = (1 - d_{t,c})\sigma_{t,c}$$

For any given cross-section of the material, the factor  $(1 - d_{t,c})$  represents the ratio of the effective load-carrying area (i.e., the overall area minus the damaged area) to the overall section area. The evolution of

the degradation variable is governed independently in tension and compression by two hardening variables:  $\tilde{\epsilon}_{t,c}^{pl} = \int \dot{\tilde{\epsilon}}_{t,c}^{pl} dt$  and the effective stress. A further detailed description of the model can be found in the ABAQUS Theory Manual version 6.4.1.

The behaviour of the reinforcement (steel bars) is modelled with an elastic ideal-plastic constitutive law with the von Mises yield condition.

## 6 FE MODELS FOR THE NUMERICAL SIMULATIONS

A seismic motion parallel to the plane of the RC frames is considered and plain strain conditions for the soil and the structure (2D-problem) are assumed. The foundation ground is defined by the soil profile for Treasure Island shown in Fig. 5. The 3-, 6-, and 12-storey buildings are founded on RC mats at a depth of 3.5 m. The mats have lengths of 7, 8 and 10m and thickness of 0.4, 0.4 and 0.8 m, respectively. Two FE models were created. The first FE model (MO-S) consists of the structure and the foundation without the soil, whereas in the second FE model (MO-SSI) the structure, the foundation and the soil are considered (Fig. 8). The RC frames are modelled with a combination of 2-node beam elements for the plain concrete and rebar elements for the reinforcement. The dimensions of the structural elements (beams and columns) as well as the diameters and location of the steel bars were chosen according to the pre-dimensioning. The soil and the foundation mat are modelled with linear (4-node) plain strain elements. The numerical simulations were carried out with the program ABAQUS version 6.4.1.

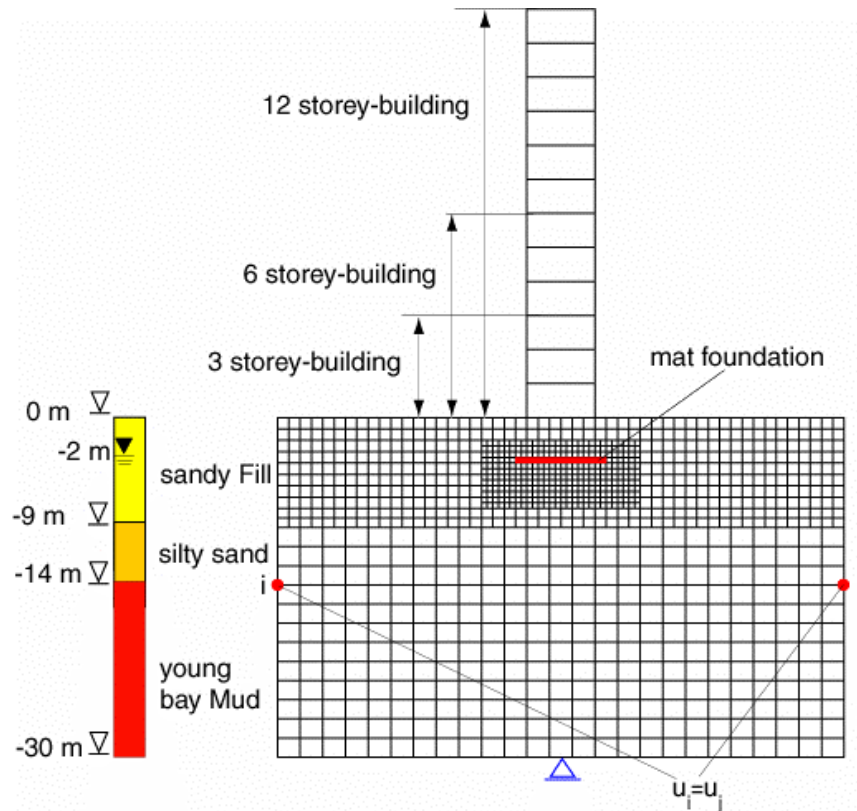


Figure 8. The MO-SSI model for the investigation of SSI. The MO-S model does not include the soil.

The MO-S model was used to simulate the dynamic linear and non linear response of the buildings subjected to the Loma Prieta 1989 earthquake, disregarding the effect of SSI. In the linear and non linear

calculations viscous (Rayleigh stiffness proportional) damping of 5% and 2.5% of the critical damping for the first mode of vibration of the buildings was assumed respectively. The horizontal motion applied to the mat foundation to simulate the earthquake was the “free field” motion calculated for 3.5 m depth with the ground response model described in section 5 (Fig. 9). The input data for the dynamic ground response analyses are the idealized soil profile for Treasure Island (Fig. 5 ) and the acceleration record for Yerba Buena Island (Fig. 6). Only the strong phase of the earthquake was considered in the FE-calculations (time window of ca. 20 s in Fig. 9). The simulations consist of two steps. In the first step, which is a static step, the gravitational loads including the weight of the structure are applied. In the second step, which is dynamic, the earthquake motion is applied.

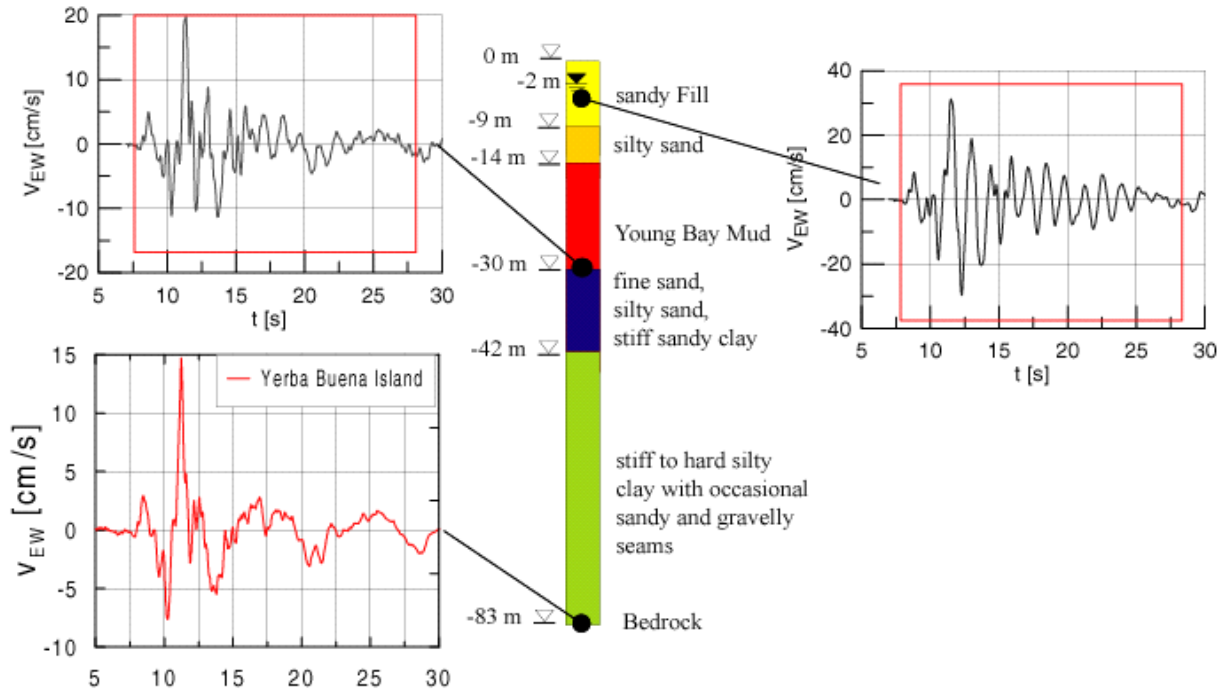


Figure 9. Calculation of the ground motion in -3.5 m and -30 m depth for Treasure Island.

The investigation of the SSI interaction was carried out with the MO-SSI model (Fig. 8). In this model the behaviour of the concrete is elastoplastic, the reinforcement is elastic-ideal plastic and the soil is hypoplastic and visco-hypoplastic. During the earthquake water drainage is not allowed for, i.e. undrained soil behaviour is assumed. The lateral boundary condition of the soil is imposed by constraining opposite nodes on these boundaries to undergo the same displacement. This boundary condition is exact for a level ground with free surface subjected to base shaking (Bühler et al.2003, Gudehus, et al. 2004), but it is still a good approximation in the case of strong earthquakes if the boundaries are located far from the foundation since under this condition radiation waves are damped before they reach the boundaries.

In order to reduce the computation time, the lower boundary of the model (base) was located at 30 m depth (Fig. 8). The earthquake was simulated by applying the horizontal seismic motion calculated for -30 m depth using the same procedure described above (Fig. 9). An additional step (step 1) is required in this case to control the initial equilibrium of the soil before the gravitational loads (step 2) and the earthquake motion (step 3) are applied. The same earthquake duration as for the calculations with MO-S are used.

## 7 RESULTS OF THE FE SIMULATIONS

The most relevant results of the FE-analyses are evaluated and discussed in this section. The names A-ELA and A-PLA refer to the results of the elastic and elastoplastic analyses with the MO-S model. The results of the calculations with the MO-SSI model are referenced as A-SSI. The 3-, 6- and 12-storey buildings are referred to as B3, B6 and B12. Fig. 10a compares the horizontal displacement of the upper floor of B3 and B12. The horizontal displacements for B6 are somewhere in between. The displacements computed in the A-ELA and A-PLA analyses are similar, indicating that in the elastoplastic analyses (A-PLA) the structures remain basically in the elastic regime. The evolution of the displacement over time in the A-SSI analysis shows longer periods and different amplitudes, especially in the second half of the earthquake. Amplitudes are smaller for B3 when considering SSI as compared to the case without SSI, whereas the contrary happens for B12.

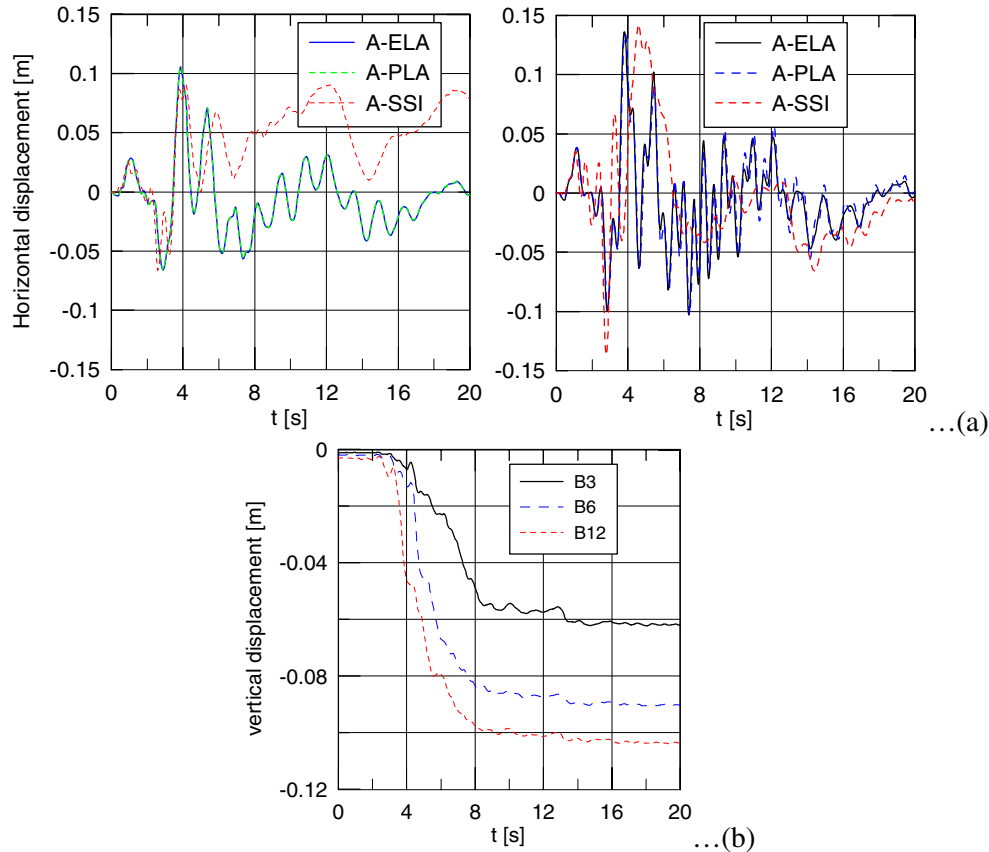


Figure 10. (a) Evolution of the horizontal displacements of the upper floor of B3(left) and B12(right); (b) evolution of the vertical displacements of the foundation of B3, B6 and B12.

As can be seen in Fig.10 and 11, the earthquake also induces permanent displacement of the buildings as a consequence of the plastic deformations of the soil. The fact that B12 settles more than B3 whereas the latter experiences larger tilting and permanent horizontal displacements cannot be generalized since the behaviour will depend on the particular characteristics of the building, the foundation and the soil. The effect of SSI on the internal forces of the structure can be evaluated with the help of Fig. 12 and 13 which compare the evolution of bending moments at the base of the 1<sup>st</sup> column and at the left border of the beam of the 1<sup>st</sup> level, respectively.

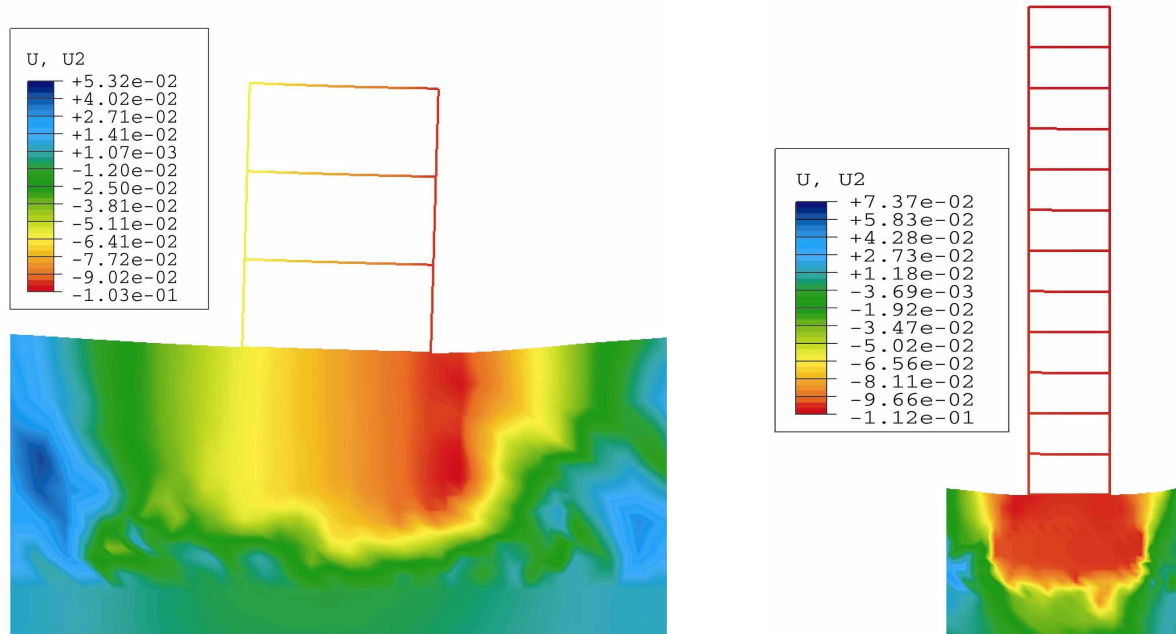


Figure 11. Distribution of vertical displacements  $u_2$  (in meters) of the structure and the soil in its neighborhood for B3 (left) and B12 (right).

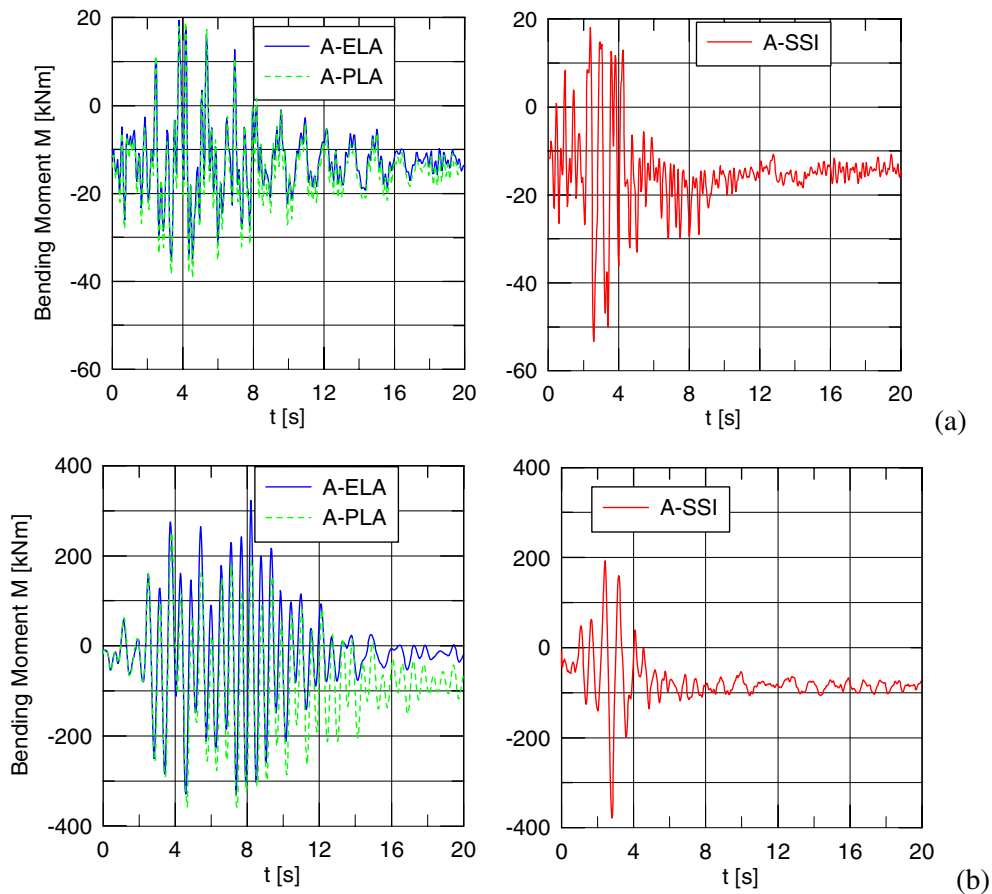


Figure 12 Evolution of the bending moment at the base of the 1<sup>st</sup> column: (a) 3-, (b) 12-storey building.

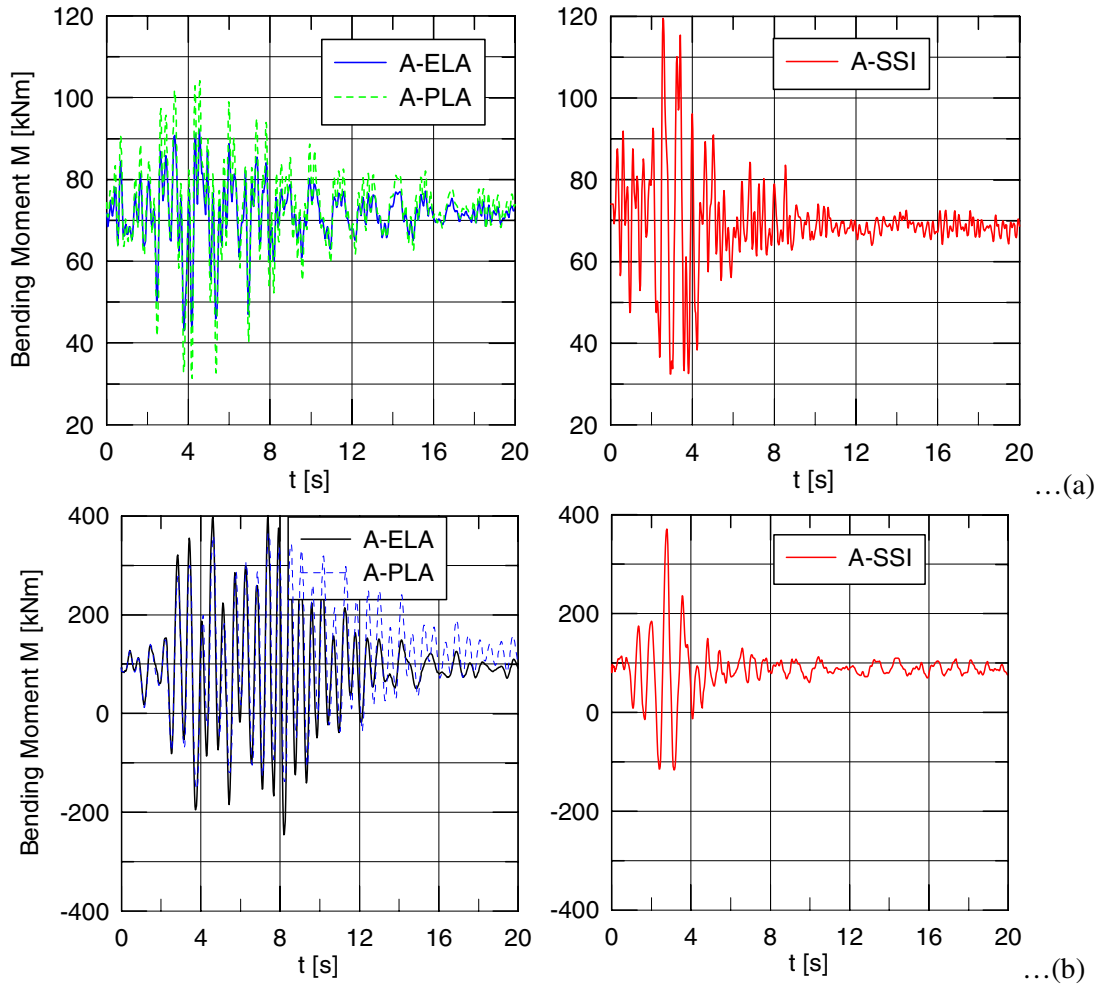


Figure 13 Evolution of the bending moment at the left border of the beam of the 1<sup>st</sup> floor (a) 3-, (b) 12-storey building.

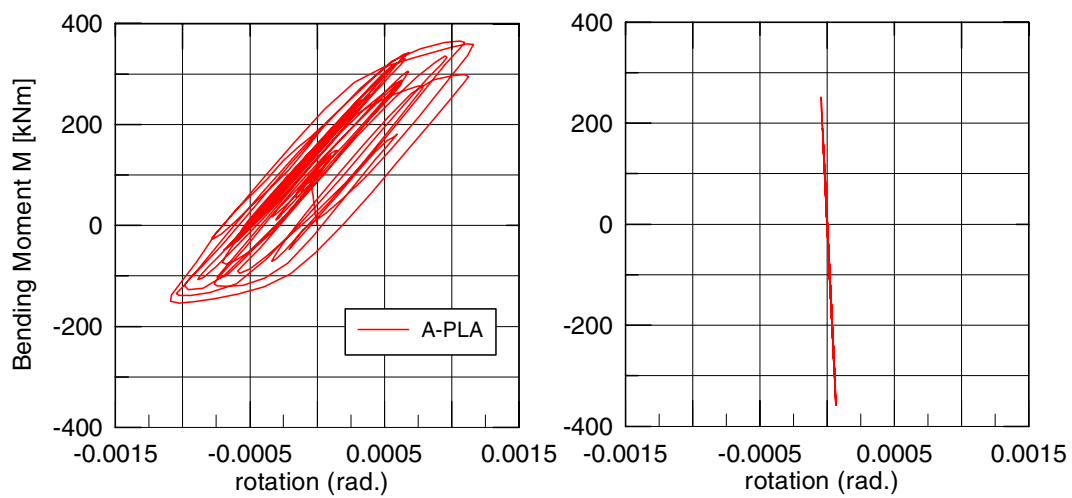


Figure 14. Bending moment vs. rotation at the border of the beam in the 1<sup>st</sup> level (left) and at the base of the 1<sup>st</sup> column (right for B12).

As in the case of the horizontal displacements, the evolution of bending moments over time for A-ELA and A-PLA are similar. In the A-PLA and A-SSI computations an increase of bending moments at the base of the buildings is observed at the end of the earthquake ( $t=20$  s) relative to the initial values for  $t=0$ , whereas no increase occurs in the elastic simulation.

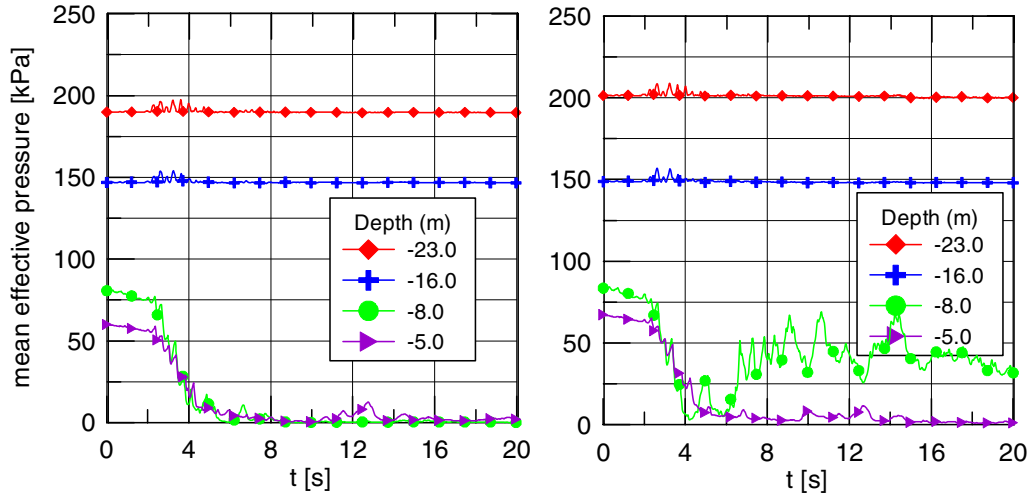


Figure 15 Evolution of the mean effective soil pressure over the time in 5.0, 8.0 and 16.0 and 23.0 m depths for B3 (left) and B12 (right).

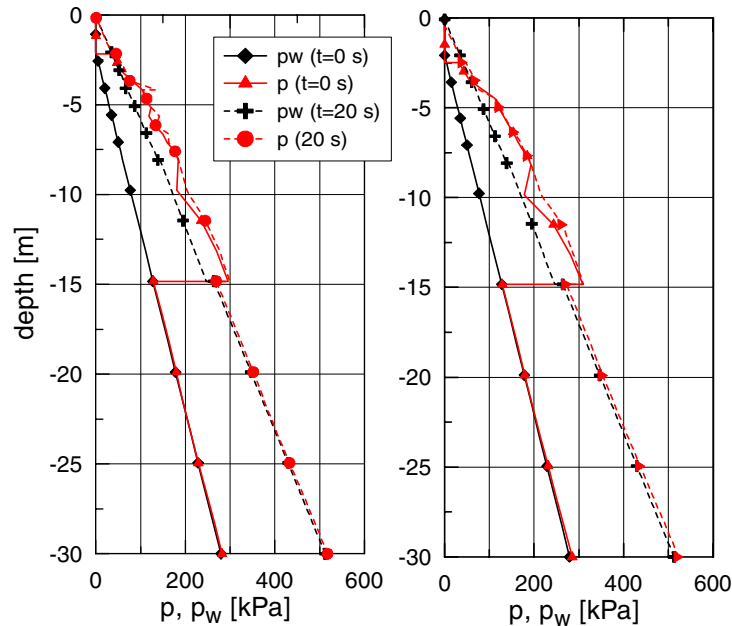


Figure 16. Distribution of mean total soil pressure and pore water pressure at the end of the earthquake in comparison with the values for the geostatic state

This change can be attributed to a redistribution of bending moments as a consequence of the plastification of tensioned zones of some beams borders which, according to the constitutive law for concrete, causes a reduction of stiffness in these zones. Note that the plastification of tensioned zones does not lead to the formation of plastic hinges because the reinforcement covers the tension demand due to the damage

of the concrete. The plastification of the beam borders can be seen in Fig. 14 which shows the non linear dependence of the bending moments on the rotation at the left border of the beam of the 1<sup>st</sup> floor computed in A-PLA. In contrast with it, the columns behaved elastically during the earthquake as shown in the same figure (similar pictures are obtained in A-SSI). The evolution of bending moments over the time changes when the SSI is taken into account. The number of loops with high bending moments reduces dramatically, .i.e. the cyclic demand is strongly overestimated when SSI is neglected. The relation between maximum bending moments with and without consideration of the SSI does not show the same tendency for B3 and B12. For B3 the maximum bending are larger, for B12 smaller when SSI is considered.

Fig 15 shows the development of the mean effective soil pressure  $p'$  during the earthquake at 5.0, 8.0, 16.0 and 23.0 m depths for buildings B3 and B12. The alternating shearing induced by the earthquake causes an important reduction of  $p'$  below the foundations of B3 and B12. 5-6 seconds after the beginning of the earthquake the effective pressures vanish, .i.e. the soil liquefies, in 5.0 m depth. Fig. 16 shows the distribution of the total mean pressure  $p$  and pore water pressure  $p_w$  over depth at the end of the earthquake as compared with the values for the geostatic state. As in the ground response analysis (Fig. 7) the reduction of  $p'$  in SSI analysis occurs only in the upper granular layers. However, in the former liquefaction concentrates in a narrow zone between 8 and 10 m in depth, whereas in the latter liquefaction extends to almost the complete layers. As opposed to granular layers, the dynamic response of the clay layer seems not to be considerably affected by the presence of the building.

## 8 FINAL REMARKS

The dynamic response of buildings founded upon soft and liquefiable soils during a strong earthquake was simulated with the FEM. The proposed numerical models take into account both the non linear behaviour of the structure and the soil realistically. The numerical results show that the design of RC structures based on the recommendations of seismic codes is extremely conservative. No plastic hinges formed in either beams or columns. Except for some tensioned zones of the beams in the lower levels, the structures behaved elastically during the strong earthquake. Consideration of SSI led to higher or lower maximum bending moments in beams and columns depending on the characteristics of the buildings. The cyclic resistance demand of the structure was always overestimated when SSI was not taken into account. Permanent displacements and tilting of the buildings, which are induced by the plastic deformations of the soil and could affect their stability or serviceability, can be also realistically predicted by the proposed numerical model.

The dynamic response of the soil is qualitatively similar but quantitatively different with and without the building. In both cases the effective stresses diminishes in the upper granular layers due to alternating shearing. However, liquefaction is more important and faster when SSI is considered, since the static loads of the building lead to higher initial effective stresses below the foundation level, and therefore to a stronger tendency of the soil to accumulate excess pore water pressure during the earthquake.

The calculations demonstrate the benefits of the *layer separation* effect for the buildings: The reduction of the effective pressure (liquefaction) causes a decrease of the shear stiffness which in turn impedes the transmission of further shear waves from the soil to the foundation of the building. Through this mechanism, which is responsible for the differences (evolution of bending and displacements, frequency content and maximum values) between the computations with and without consideration of SSI, a liquefiable soil could provide a natural and effective isolation for a building if its stability and serviceability thereby are not endangered.

The proposed numerical models can be applied to the investigation of SSI problems involving other structures, foundations and soils types.

## REFERENCES

1. ABAQUS Theory Manual version 6.4.1.
2. Bühler M.M., Cudmani R.O., Osinov V.A., Librerios-Bertini A.B., Gudehus G. (2003). "Experimental and numerical investigation of the influence of local site conditions on the ground motion during strong earthquakes. Geotechnical Measurements and Modelling, Balkema, p. 441-449.
3. Cudmani R.O., Osinov V.A., Bühler M.M., Gudehus G. (2003). "A Model for the Evaluation of Liquefaction Susceptibility in Layered Soils Due to Earthquakes". 12<sup>th</sup> Panamerican Conference on Soil Mechanics and Geotechnical Engineering, Vol. 1, p. 969-976.
4. Cudmani R.O., Osinov V.A. (2001) "The cavity expansion problem for the interpretation of cone penetration an pressuremeter tests". Canadian Geotechnical Journal 38, p. 622-638.
5. Gudehus G., Cudmani R.O., Librerios-Bertini A.B., Bühler M.M. (2003). "In-plane and anti-plane strong shaking of soil systems and structures". Soil Dynamics and Earthquake Engineering, accepted for publication.
6. Herle I., Gudehus G. (1999). "Determination of parameters of hypoplastic constitutive model from properties of grain assemblies". Mechanics of Cohesive-Frictional Materials, 4 (5), p. 461-486.
7. Mylonakis G., Gazetas G. (2000). "Seismic Soil-Structure Interaction: beneficial or detrimental?". Journal of Earthquake Engineering, Vol. 4, No. 3, p. 277-301.
8. Niemunis A., Herle I. (1998). "Hypoplastic model for cohesionless soils with elastic strain range". Mechanics of Cohesive-Frictional Materials, 4 (2), p. 279-299.
9. Niemunis A. (2003). "Extended Hypoplastic model for Soils". Habilitation Thesis. No. 34. Institute of Soil and Rock Mechanics, University of Bochum.
10. Osinov V.A. (2000). "Wave-induced liquefaction of a saturated sand layer". Continuum Mechanics and Thermodynamics, 12 (5), p. 325-339.
11. Osinov V.A. (2003). "A numerical model for the site response analysis and liquefaction of soil during earthquakes". Geotechnical Measurements and Modelling, Balkema, p. 475-481.
12. Pralle N., Gudehus G. (2000). "Compaction of loose flooded granular masses using air pulses". In: Kolymbas D., Fellin W., editors. Compaction of soils, granulates and powders. Advances in geotechnical engineering and tunnelling, Balkema, Vol. 3, p. 207-231.
13. Reglamento INPRES-CIRSOC 103 (1983). "Normas Argentinas para las Construcciones Sismo-resistentes. Parte I: Construcciones en General, Parte II: Construcciones de Hormigón Armado y Hormigón Pretensado, Parte III: Construcciones de Mampostería". Ed. por el INTI (Instituto Nacional de Tecnología Industrial). Buenos Aires, Argentina.
14. Reglamento INPRES-CIRSOC 103 (1991). "Normas Argentinas para las Construcciones Sismo-resistentes". Nueva Edición, ed. por el INTI (Instituto Nacional de Tecnología Industrial). Buenos Aires, Argentina.
15. Seed R.B., Dickenson S.E., Idriss I.M. (1991). "Principal geotechnical aspects of the Loma Prieta earthquake". Soil and Foundations, 31 (1), p. 1-26.
16. Zienkiewicz O.C., Chang C.T., Bettess P. (1980). "Drained, undrained, consolidating and dynamic behaviour assumptions in soils". Géotechnique, 30 (4), p. 385-395.
17. Zienkiewicz O.C., Chan A.H.C., Pastor M., Schrefler B.A., Shiomi T. (1999). "Computational geomechanics with special reference to earthquake engineering". Chichester, Wiley.
18. Lee, J., and G. L. Fenves, "Plastic-Damage Model for Cyclic Loading of Concrete Structures," Journal of Engineering Mechanics, vol.124, no.8, pp. 892-900, 1998.
19. Lubliner, J., J. Oliver, S. Oller, and E. Oñate, "A Plastic-Damage Model for Concrete," International Journal of Solids and Structures, vol.25, no.3, pp. 229-326, 1989.